JPE 19-1-1

https://doi.org/10.6113/JPE.2019.19.1.1
ISSN(Print): 1598-2092 / ISSN(Online): 2093-4718

Novel Single-inductor Multistring-independent Dimming LED Driver with Switched-capacitor Control Technique

Guozhuang Liang* and Hanlei Tian†

†,*School of Electrical Engineering, Hebei University of Science and Technology, Shijiazhuang, China

Abstract

Current imbalance is the main factor affecting the lifespan of light-emitting diode (LED) lighting systems and is generally solved by active or passive approaches. Given many new lighting applications, independent control is particularly important in achieving different levels of luminance. Existing passive and active approaches have their own limitations in current sharing and independent control, which bring new challenges to the design of LED drivers. In this work, a multichannel resonant converter based on switched-capacitor control (SCC) is proposed for solving this challenge. In the resonant network of the upper and lower half-bridges, SCC is used instead of fixed capacitance. Then, the individual current of the LED array is obtained through regulation of the effective capacitance of the SCC under a fixed switching frequency. In this manner, the complexity of the control unit of the circuit and the precision of the multichannel outputs are further improved. Finally, the superior performance of the proposed LED driver is verified by simulations and a 4-channel experimental prototype with a rated output power of 20 W.

Key words: Circuit analysis, Electromagnetic interference (EMI), Load sharing, switched capacitor, Voltage source converters

I. INTRODUCTION

Lighting accounts for a large proportion of human energy consumption [1]. As a new generation of green lighting, LED is widely used invisible light communications, UV LED, transportation, and similar applications because of its high efficiency, small losses, and wide color gamut [2]-[4]. Given the power limitation of a single LED load, a considerable number of LEDs must be used in series and parallel connections for obtaining sufficient luminance [5].Current unbalance occurs if the driver does not have a current balancing mechanism when multiple arrays of LEDs are driven in parallel. A large current can be developed in some LED strings, there by accelerating aging and failures, which affect the lifespan and stability of the entire LED system. Therefore, research on multichannel current sharing is important.

Manuscript received Feb. 9, 2018; accepted Aug. 16, 2018
Recommended for publication by Associate Editor Il-Oun Lee.
†Corresponding Author: THLedu@163.com
Tel: +86-18729227236, Fax: +86-0311-81668724
*School of Electrical Eng., Hebei Univ. of Sci. and Technol., China

To solve the above problems, active and passive approaches have been proposed [6]-[14]. The active approach in [6] connects either a linear-mode or a switched-mode current regulator to each LED string to achieve precise current sharing and independent control.

Each array requires a separate control and driving circuit, which increasing structural complexity, cost, and losses [7]. In view of the disadvantages of active current sharing, the capacitance and inductance of passive components have been utilized for realizing current sharing [8]-[14]. According to the theory of electromagnetic coupling, such coupling components as coupled inductors and transformers are adopted for achieving the current sharing of multiple strings. Compared with active current sharing, passive sharing has been optimized in terms of the number of components and the complexity of control circuits [8]. However, high cost is still an issue due to the exponential growth of magnetic inductors with the increased number of LED strings. In addition, the efficiency of LED drivers is reduced due to increased core losses. Subsequently, the daisy-chained structure was improved and applied to decrease coupling inductor and conduction loss in [9], [10]. Sharing accuracy is generally affected by the

coupling coefficient. Thus, the capacitance-impedance balance was presented; the approximate balance between each string is realized by the capacitance impedance's substantially larger size than that of the internal resistance of the LED channel [11]. In practice, the high accuracy of current sharing is penalized due to the impedance difference. Furthermore, a large impedance indicates a high voltage drop in the lighting system. Compared with the impedance balance of capacitors, the charge balance of trans-conduction capacitors has better current sharing [12]. However, many existing switches are under hard switching. Therefore, they can run at low frequencies only, and the volume of their driver is limited. For enhanced transmission efficiency, a high-order resonant network is utilized, and soft switching is realized by sacrificing power density [13]. However, the use of current sharing capacitors at resonant tanks for structural simplicity in high-frequency operation leads to the capacitance drift that results in LED flicker, which can harm the eyes [14].

In addition to current sharing, dimming capability is significant to LED lighting applications, but the structure of dimmable circuits is complicated and not highly reliable at present [15]. Resonant elements are used to adjust brightness, and PWM dimmable circuits are eliminated by variable inductance (VI), which greatly improves the cost of dimming circuits [16]. However, an extra winding and control system is added to regulate the VI, which leads to a complicated structure and increased cost. Magnetic elements also have more core loss and a larger volume, so switched-capacitor control (SCC) was used in [17], and the duty cycle is adjusted to suit the variable load. Some cases have different brightness requirements where independent dimming cannot be realized [18]. In another case, SCC was applied to an inductance-inductance-capacitor (LCC) resonant converter to obtain dimming capability [19]. However, the LCC resonant circuit had low efficiency under light-load conditions. Although an LCL&LLC resonant converter combined with an SCC unit can realize relatively high efficiency, it also has noticeable shortcomings in cost and volume [20].

To overcome the problems presented in the above topologies, such as fixed frequency, high accuracy of current sharing, and parameter drift of resonators, a novel multichannel, independent dimming LED driver is proposed in this work. The individual dimming capability of each string based on SCC is simple and reliable for a wide range of load variations. In addition, its current sharing capability has high efficiency while maintaining low cost.

The remainder of this paper is organized as follows. Topology analysis is shown in Section II. In Section III, an intensive analysis of the current sharing scheme is presented. In Section IV, the new dimming approach, which is based on SCC, is discussed. The design of the parameters is presented in Section V. Performance evaluation, including PSIM simulations and experimental analysis, are presented in Section VI. The conclusions drawn are presented in Section VII.

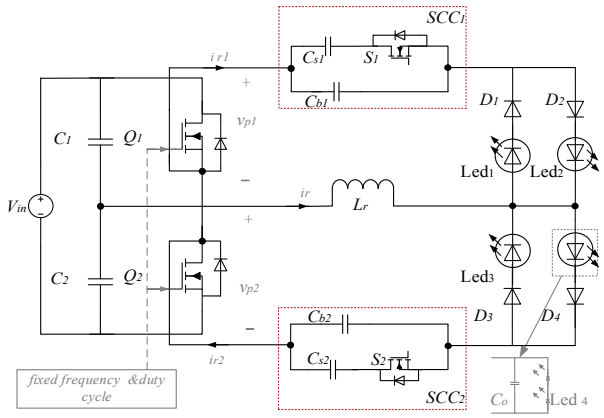

Fig. 1. Proposed multichannel LED driving circuit.

TABLE I
COMPONENT COMPARISON

	Number of output strings	MOSFET	Inductor	Current sharing type	Independent dimming
[21]	n	2	Two	Capacitance impedance	No
[19]	n	n+2	Single	Capacitance impedance	Yes
[18]	n	n/2+2	n/2+1	Capacitance charge	Yes
Proposed	n	n/2+2	Single	Capacitance charge	Yes

II. TOPOLOGY ANALYSIS

As shown in Fig. 1, the proposed circuit is used for the current sharing of four-channel outputs. It consists of a voltage-fed half-bridge (C_2, C_1, V_{in}, Q_1, and Q_2) and a resonant unit, including an inductor L_r, two SCC units (SCC_1 and SCC_2) and four rectifier units (LED_i, diodes $D_{1\text{-}4}$ and the output capacitor C_o). Led_i (i = 1, 2, 3, 4) represents the LED channel, D_1–D_4 are the rectifier diodes, and each SCC unit consists of two capacitors (C_{s1} and C_{b1}, C_{s2} and C_{b2}) and one switch (S_1 and S_2).

The proposed driver can be equivalent to two resonance networks, with the sharing of the voltage-fed half-bridge and the inductor (L_r), such that only a single inductor is realized. To simplify the circuit structure and improve the stability of the system, SCC_i (i = 1, 2) meanwhile plays the roles of resonance, current balancing, and dimming. The series resonance between L_r and SCC_i (i = 1, 2) can generate a sinusoidal current (i_r), and the half-bridge generates two separate outputs (v_{p1} and v_{p2}) for the upper and lower arms. Multistring outputs are voluntarily current sharing due to the charge balance of SCC_i.

A comparative analysis of the LED drivers is summarized in Table I, including the number of active switches, the number of inductors, the sharing method, and the dimming strategy.

Comparisons with existing topologies show that the proposed

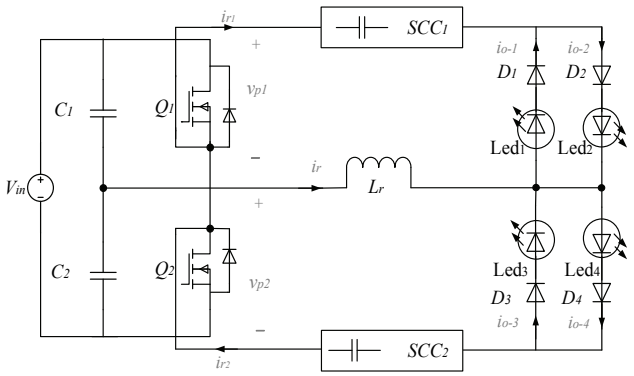

Fig. 2. Simplified version of the proposed LED driver.

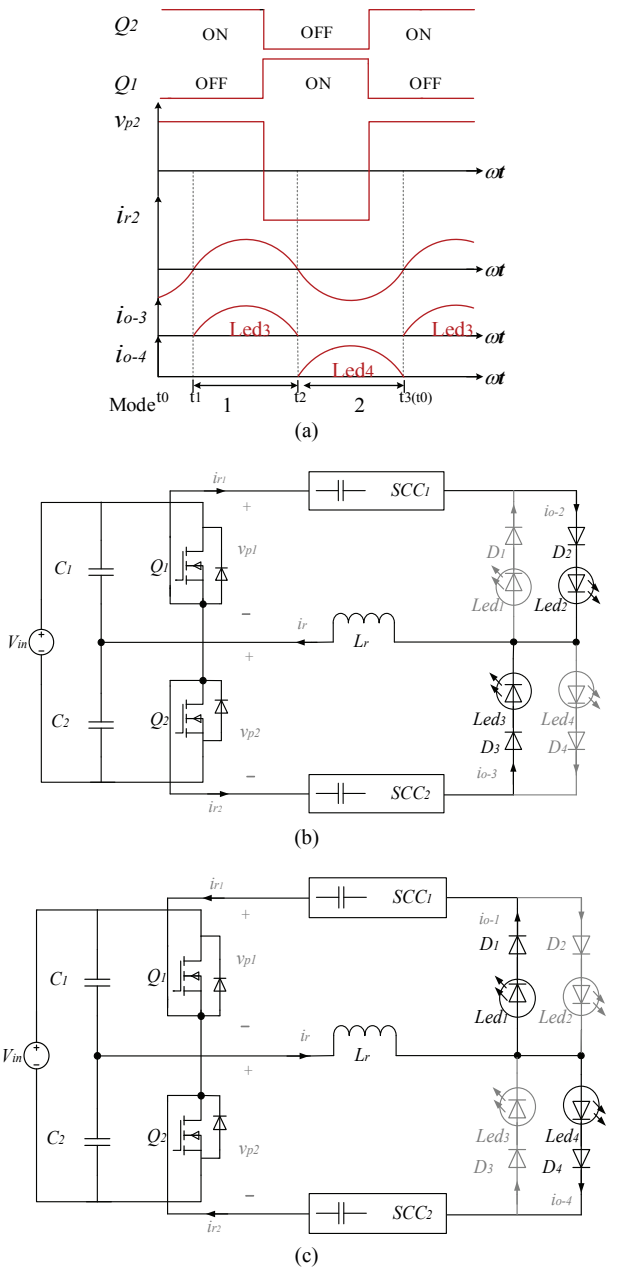

Fig. 3. Steady state: (a) Theoretical operation waveform; (b) Steady-state Mode 1: t1–t2; (c) Steady-state Mode 2: t2–t3.

topology has the highest power density because the voltage-fed half-bridge and inductor L_r are shared for the front and rear stages. Meanwhile, a wide range of dimming regulation is accomplished by the SCC with high reliability. Given that the capacitive charge balance is used for current sharing among the different LED branches, high-precision current sharing is achieved with the proposed topology. Meanwhile, an additional active switch is required for the SCC dimming unit. However, the cost increase of the proposed circuit is limited for the LED output of multiple strings.

III. Current Sharing Analysis

A. Current Sharing of Branches

The current sharing principle is adopted by simplification of the circuit presented in Fig. 2, where SCC_i is simplified as capacitors C_{eq1} and C_{eq2}. Meanwhile, the dead time caused by the charging and discharging operations is ignored at the ends of switches Q_1 and Q_2. Fig. 3(a) illustrates the theoretical waveforms of the lower half-bridge due to the symmetrical feature. In addition, Figs. 3(b) and 3(c) show the operation modes during one switching cycle, where the current through each string is defined as $i_{o\text{-}i}$ (i = 1, 2, 3, 4).

Fig. 3(a) shows that capacitor C_{eq2} is charged at t_1–t_2 and discharged at t_2–t_3 under each switching cycle. On the basis of the principle of the capacitive charge balance, the equation can be expressed as

$$Q_{\text{ch}} = \int_{t2}^{t1} i_{r2}(t)d(t) = \int_{t3}^{t2} i_{r2}(t)d(t) = Q_{dis} \,. \tag{1}$$

According to the above analysis, Eq. (1) can synchronously be applied to Led_1 and Led_2, and i_{r2} should be replaced by i_{r1}.

B. Current Sharing of the Upper and Lower Half-bridges

The static equivalent model of the lower half-bridge is illustrated in Fig. 4, where v_{p1} and v_{p2} are obtained by the half-bridge part and have the same amplitude, with a phase difference of 180° during each switching cycle. Hence, the voltage v_p is utilized for showing the fundamental component of the half-bridge output.

The peak value of the fundamental component is acquired by Fourier transformation.

$$V_p = \frac{4V_{\text{in}}/2}{\pi} = \frac{2V_{in}}{\pi} \tag{2}$$

An ideal LED channel is replaced by an electrical model that consists of the threshold voltage V_{LED} and the resistance R_{LED} [22]. Therefore, the equivalent resistance R_{eq} is presented below.

$$R_{eq} = \frac{V_{LED} + R_{LED} \times I_{o\text{-}LED}}{I_{o\text{-}LED}} = \frac{V_{o\text{-}LED}}{I_{o\text{-}LED}} \,, \tag{3}$$

where the output voltage and output current of the LEDs are $V_{o\text{-}Led}$ and $I_{o\text{-}Led}$, respectively, and the AC equivalent resistance

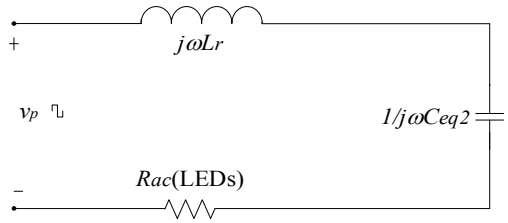

Fig. 4. Equivalent impedance model of the lower half-bridge.

R_{ac} is expressed as $8R_{eq}/\pi^2$. The loop impedance Z_{LED} is obtained by an analysis of Fig. 4.

$$Z_{LED} = 1/\, j\omega C_{eq2} + j\omega L_r + R_{ac} \tag{4}$$

Thus, the current passing through the resonant tank is i_{r2}, and the peak value is I_{r2}.

$$\begin{aligned} I_{r2} &= \frac{V_p}{R_{ac} + j(\omega L_r - 1/\omega C_{eq2})} \\ &= \frac{V_{p2\text{-}p}}{\sqrt{8R_{LED}^2/\pi^2 + j(\omega L_r - 1/\omega C_{eq2})}} \end{aligned} \tag{5}$$

The equivalent resistance R_{ac} is negligible when compared with the capacitive impedance. Therefore, Eq. (5) is simplified as

$$I_{r2} = \frac{V_p}{\mathrm{j}\omega L_r - 1/\, j\omega C_{eq2}}. \tag{6}$$

This current is rectified and filtered by the diodes and output capacitor C_o. Therefore, the output current $I_{o\text{-}LED}$ is obtained by

$$I_{o-LED} = \frac{2 \,||\, I_{r2} \,||}{\pi}. \tag{7}$$

From the above analysis, the peak current of the upper bridge (I_{r1}) is obtained and presented below.

$$I_{r1} = \frac{V_p}{j\omega\omega_r - 1/j\omega C_{eq1}} \tag{8}$$

Provided that S_1 and S_2 have the same duty cycle, the equationC_{eq1}=C_{eq2} must be satisfied where all the capacitors are assumed to not exist in tolerance [23]. Given that L_r is shared for the upper and lower bridges, the average current $I_{a\text{-}LED}$ of LEDs can be derived by

$$I_{a\text{-}LED} = \frac{\int_0^{\pi} I_{r1}\sin(t)dt}{\pi} = \frac{\int_0^{\pi} I_{r2}\sin(t)dt}{\pi}. \tag{9}$$

Consequently, multichannel current sharing is achieved with less reactive power than with current sharing based on impedance matching.

IV. Dimming Control

A. Operational Cycles of SCC

Given the symmetry of characteristics, the resonant unit of only the lower half-bridge is discussed in detail. Dimming is accomplished by an SCC unit, as shown in Fig. 5, where sinusoidal current i_{r2} flows from point A to point B.

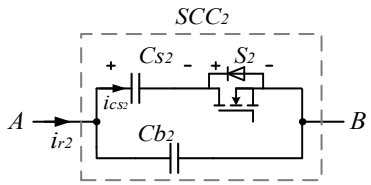

Fig. 5. Schematic of SCC_2.

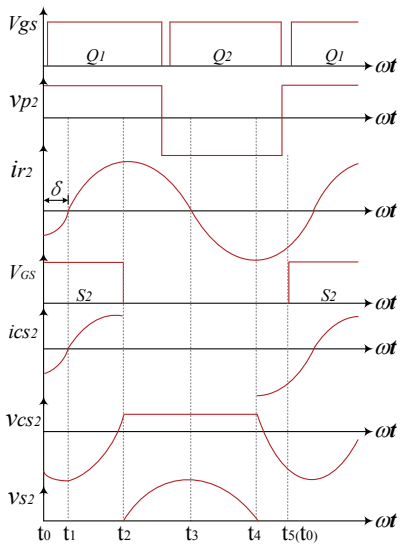

Fig. 6. Waveforms of the SCC_2 operational cycle.

The theoretical waveforms of SCC_2 are shown in Fig. 6, where δ is a phase angle and voltage v_{p2} leads current i_{r2}. In addition, the time interval is t_δ, which achieves ZVS for the main switches (Q_1 and Q_2) and S_1 and S_2, where $t_\delta = \delta/\omega_s$ ($\omega_s = 2\pi f_s$). The current (i_{cs2}) flows into the capacitor (C_{s2}). The voltage across capacitor C_{s2} is v_{cs2}, and v_{s2} is the voltage over switch S_2.

[t_0–t_1]: Switch S_2 is triggered at t_0. The current i_{cs2} flowing into L_r freewheels through the anti-parallel diode of switch S_2. Capacitor C_{s2} is reversely charged due to the body diode, and the voltage across switch S_2 is clamped to zero.

[t_1–t_2]: At t_1, switch S_2 is subjected to ZVS. Besides, the chopper voltage of the half-bridge is linked to a resonant tank, comprising C_{s2}, C_{b2}, and L_r. Voltage v_{cs2} is reversely charged to the maximum and discharged at t_1.

[t_2–t_3]: Switch S_2 turns off with soft switching at t_2. Besides, the voltage of capacitor C_{s2} remains at the maximum value. During this operating moment, capacitor C_{b2} is charged by i_{r2}. The resonant frequency in this interval is obtained by

$$f_r = \frac{1}{2\pi\sqrt{C_{b2}\times L_r}}. \tag{10}$$

[t_3–t_4]: Current i_{cs2} flows through zero from positive to negative at t_3. In addition, the voltage across switch S_2

decreases with the discharge of capacitor C_{b2}. The resonant frequency in this interval is obtained by

$$f_r = \frac{1}{2\pi\sqrt{(C_{b2}+C_{s2})L_r}}. \quad (11)$$

[t_4–t_5]: Current i_{cs2} continues to freewheel through the body diode of switch S_2. At this stage, the voltage across switch S_2 is clamped to zero. This mode finishes at t_5 when MOSFET S_2 newly obtains the trigger signal. Then, the above cycle [t_0–t_5] is repeated.

B. Dimming Analysis

The charge amount of Q is proportional to the capacitance during one cycle [24].Thus, the equivalent capacitance of SCC_2 is deduced as follows.

$$C_{s\text{-}2} = \frac{1-\cos[2\pi(D_{s2}-\delta/180)]}{2} C_{s2} \quad (12)$$

where

D_{s2} - duty cycle of S_2
Q_{s2} - capacitor charge of C_{s2}
$C_{s\text{-}2}$ - variable capacitance of SCC_2 adjustment

C_{b2} is the constant. Therefore, the equivalent capacitance of SCC_2 is

$$\begin{aligned} C_{eq2} &= C_{b2} + C_{s\text{-}2} \\ &= C_{b2} + \frac{1-\cos[2\pi(D_{s2}-\delta/180)]}{2} C_{s2} \end{aligned}. \quad (13)$$

The maximum value of duty cycle is $D_{s2\text{-}max}$ and less than 0.9 due to the margin considerations [25]. Meanwhile, the duty ratio D_{s2} is regulated by the feedback control. Thus, the equivalent capacitance of the SCC_2 unit is influenced by the adjustment of D_{s2}. The voltage gain between the input and output voltages is determined by the ratio of switching frequency f_s to resonant frequency f_r. When the switching frequency maintains a fixed value, the adjustment of the resonant frequency can perform output control. Thus, dimming is achieved with constant frequency operation. According to Eqs. (8) and (13), the relations between output current $I_{o\text{-}LED}$ and duty ratio D_{s2} is plotted in Fig. 7 for different values of V_{in}.

The figure shows the following. 1) The output current declines with the increase of duty ratio D_{s2}. 2) When D_{s2} varies within the range of 0.3 to 0.6, the regulation capability of D_{s2} to the output current weakens. 3) The output current is continuously changed from 98mA to 0.67 A. Therefore, LED dimming can be accomplished with a fixed frequency.

For attenuating the slope in Fig. 7 and increasing the precision of dimming, the value of C_b should be slightly larger than the value of C_s. In addition, the upper and lower half-bridges can separately control the multichannel outputs because they have the same control strategy. Hence, Fig. 7 can also be applied to the SCC_1 unit.

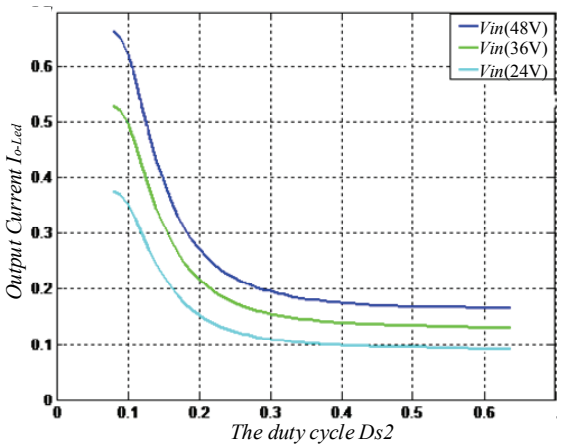

Fig. 7. Output current versus duty cycle D_{s2}.

V. Design Considerations

After the desired running point of the resonant network is identified, the design procedures of component parameters are summarized as follows.

Step 1: The required capacitance from $C_{eq\text{-}min}$ and $C_{eq\text{-}max}$ is chosen for meeting a wide range of dimming. C_s and C_b are determined to be 220 and 190 nF via Eqs. (12) and (13). Thus, $C_{eq\text{-}min}$ and $C_{eq\text{-}max}$ are 220 and 410 nF, respectively.

Step 2: To remain insensitive to the variations of output capacitor C_o and consider its corresponding dynamics, the PSIM platform is used to check the design on the basis of Eq. (14). Finally, the value of C_o is set to 50 uF.

$$f_r = \frac{1}{2\pi\sqrt{\frac{C_{eq}\times C_o}{C_{eq}+C_o}L_r}} \approx \frac{1}{2\pi\sqrt{C_{eq}L_r}} \quad (14)$$

Step 3: The minimum value of the power factor correction voltage is set to 90 V, delivering an LED current of 1.5 A (365mA × 4). Thus, voltage gain M_v is set to 2. According to [18], M_v is expressed as follows.

$$M_v = \frac{2X_{Ceq}}{X_{Lr}}, \quad (15)$$

where

$$X_{Ceq} = \frac{1}{2\pi\times f_s C_{eq}}, \quad (16)$$

$$X_{Lr} = 2\pi\times f_s L_r. \quad (17)$$

The corresponding X_L can be expressed as

$$L_r = \frac{X_{Lr}}{2\pi\times f_s C_{eq}}. \quad (18)$$

On the basis of Eq. (18), inductor L_r is set to 55 μF at a fixed switching frequency.

Step 4: For the sake of the requirements of softs witching, the switching frequency should be slightly larger than the maximum resonant frequency $f_{r\text{-}max}$ and satisfy Eq. (19). Therefore, $0.8C_{eq}$ is considered and used in Eq. (20). The

CCM operation of the resonance current should be noted. Thus, frequency f_s is finally set to 70 kHz by the tradeoff in the PSIM platform.

$$f_s \geq f_r \tag{19}$$

$$f_s = \frac{1}{2\pi\sqrt{0.8C_b \times L_r}} \tag{20}$$

VI. Performance Evaluations

A. Simulation Analysis

For verification of feasibility, the proposed LED driver is assessed on the PSIM platform with four-channel LED outputs. A simulation prototype is presented in Fig. 8, and different output impedances are chosen for the performance assessment of current sharing, where each ideal LED is a diode, a threshold voltage (approximately 3 V), and a resistance (0.6 Ω) in series [26].

The component parameters are displayed in Table II, and the simulation waveforms of the key points are shown in Figs. 9 and 10.

$V_{GS\text{-}S1}$ and $V_{GS\text{-}S2}$ are the trigger signals of S_1 and S_2, respectively. Fig. 9 shows that the trigger signals are provided while currents i_{r1} and i_{r2} are negative through S_1 and S_2. Therefore, the anti-parallel diodes of S_1 and S_2 are in the conduction state and ensure the realization of ZVS.

Fig. 10(a) shows the dynamic process where the duty cycle of the SCC unit D_s is adjusted from 0.9 to 0.2. In addition, the fast start-up time and the quick adjustment time are presented. Stable current sharing is realized, as presented in Fig. 10(b); the slope is steep, ranging from 0.12 to 0.15, and a large dimming range is realized.

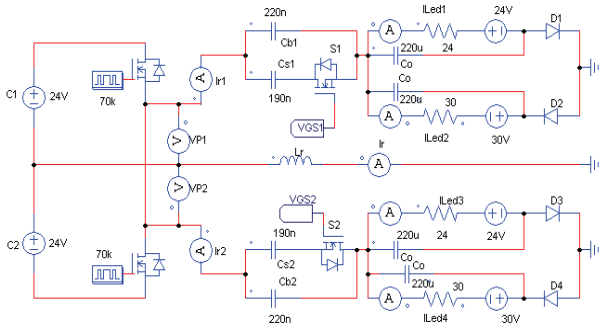

Fig. 8. Simulation circuit under PSIM.

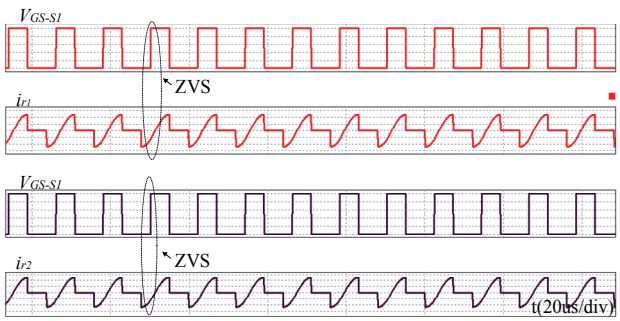

Fig. 9. ZVS characteristics of the SCC unit.

TABLE II
Key Components of the Prototype

Parameters	*Values*	*Parameters*	*Values*
V_{in}	48 V	L_r	55 μH
f_s	70 kHz	C_o	50 uF/220 V
C_{b1}, C_{b2}	220 nF/220 V	Q_1, Q_2, S_1, S_2	IRF540N (23 A/100 V)
C_{s1}, C_{s2}	190 nF/220 V	D_1~D_2	SR560-T (15 A/60 V)

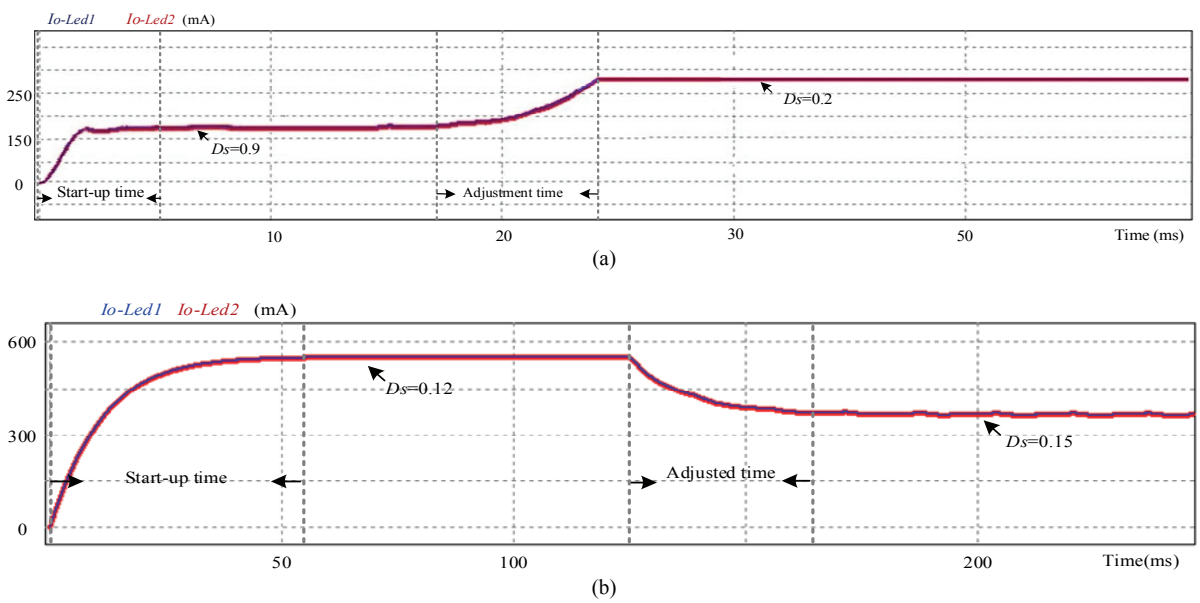

Fig. 10. Dynamic adjustment process of the SCC unit: (a) D_s from 0.9 to 0.2; (b) D_s from 0.12 to 0.15.

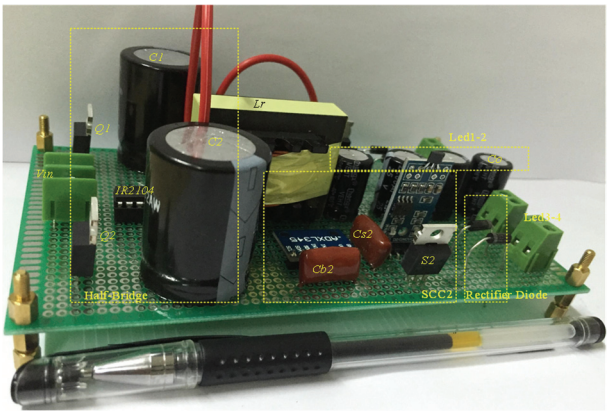

(a)

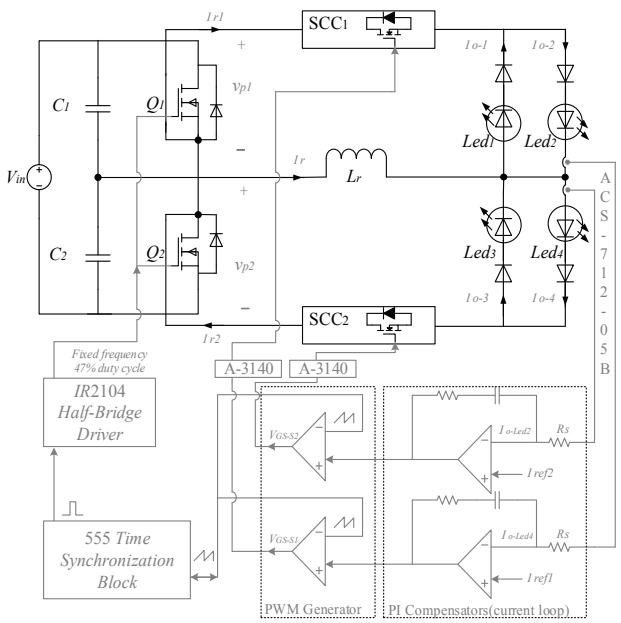

(b)

Fig. 11. Experimental prototype and control unit: (a) Photograph of the experimental prototype; (b) Control unit of the experimental prototype.

B. Experimental Verifications

The experimental prototype shown in Fig. 11(a) is built with approximately 20W. Moreover, Cree XLamp XR-E series LEDs are employed; string 1 (Led1) has five lamps, string 2 (Led2) has ten lamps, string 3 (Led3) has nine lamps, and string 4 (Led4) has fourteen lamps.

The control unit is demonstrated in Fig. 11(b), where R_s is the sampling resistor, and sampling currents $I_{o\text{-}Led2}$ and $I_{o\text{-}Led4}$ are obtained by a hall-sensor ACS-712-05B. Fig. 11(b) indicates that output current $I_{o\text{-}Led}$ is controlled by the corresponding control loop, which compares sampling currents $I_{o\text{-}Led2}$ and $I_{o\text{-}Led4}$ to references I_{ref1} and I_{ref2}. Moreover, the error signal is compensated by the PI compensator and modulated by the PWM generator to provide the control signals of S_1 and S_2. In addition, the half-bridge driver is an IR2104 operating at a fixed frequency and a duty cycle of 47% due to the dead time. Furthermore, the half-bridge switches and S_1 and S_2 are synchronized by a 555 Timer operating in a stable state. The experimental parameters are consistent with the simulation parameters, and the specific devices and instruments are listed in Table III.

TABLE III
INSTRUMENTS AND COMPONENTS USED IN EXPERMENT

Type	Symbol	Model
Device	Half-bridge driver	IR2104
	Diode	SR560
	Inductor	Ferrite core
	Optocoupler	A-3140
	DC voltage source	TDGC2

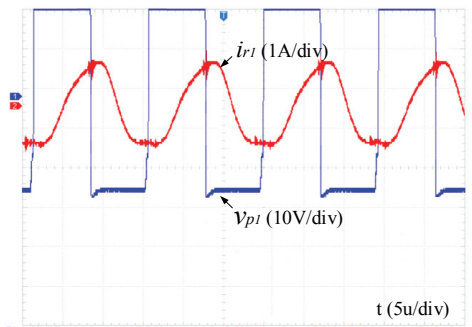

(a)

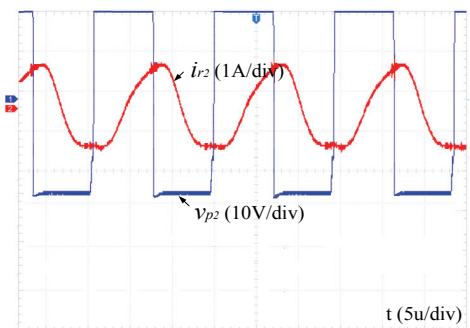

(b)

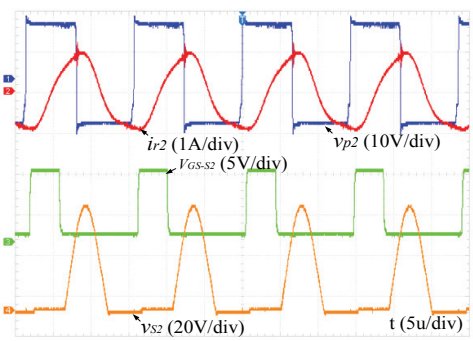

(c)

Fig. 12. Soft-switching characteristics of LED drive circuit: (a) Upper half-bridge; (b) Lower half-bridge; (c) SCC_2 unit.

Figs. 12(a) and 12(b) show the measured waveforms of output voltages v_{p1} and v_{p2} and resonant currents i_{r1} and i_{r2}, respectively. From Figs. 12(a) and 12(b), the entire circuit works in the inductive area to ensure the ZVS operation of Q_1

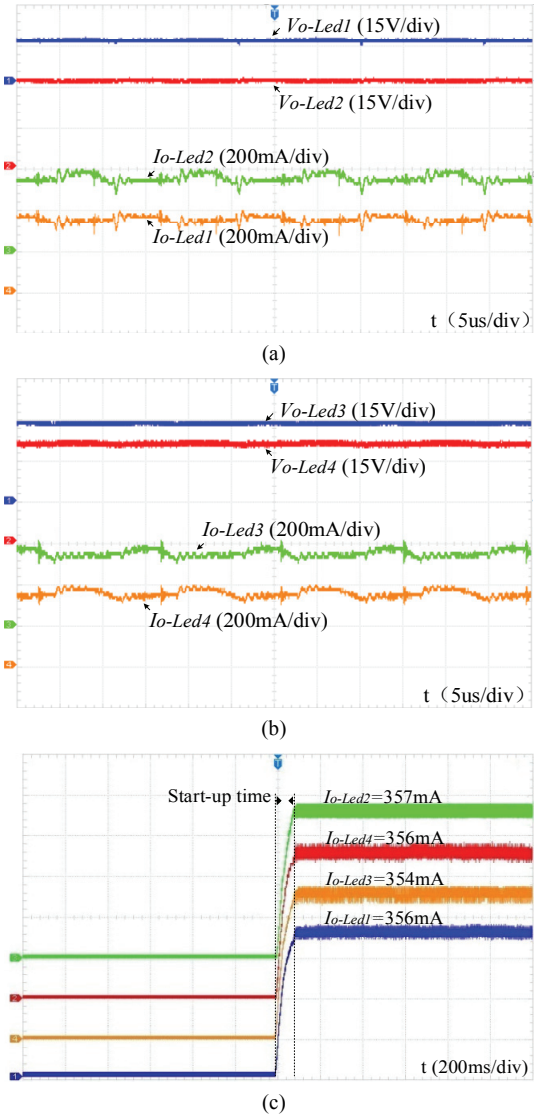

Fig. 13. Current sharing verification of the four LED strings: (a) Two channels of the upper half-bridge; (b) Two channels of the lower half-bridge; (c) Four channels.

and Q_2. When compared with driving voltage $V_{GS\text{-}S2}$ and voltage v_{s2}, the ZVS of MOSFET S_1 can be verified by Fig. 12(c). Thus, the proposed topology can achieve ZVS for SCC_2 as well, and small loss and high efficiency can be achieved.

The voltages of string 1 $V_{o\text{-}Led1}$ and string 2 $V_{o\text{-}Led2}$ are illustrated in Fig. 13(a). The voltages of string 3 $V_{o\text{-}Led3}$ and string 4 $V_{o\text{-}Led4}$ are shown in Fig. 13(b). The output voltages of the LEDs vary due to the different numbers of LEDs in each string. Fig. 13(c) shows the experimental waveforms of the four output currents, where D_{S1} and D_{S2} are 0.17. The output current of the four paths is good due to the capacitive charge balance, and the value is approximately 360 mA. In addition, this finding verifies the feasibility of superimposing the upper and lower half-bridges to the outputs. In practice, capacitor C_o is not infinitely large. Therefore, current ripple is inevitable.

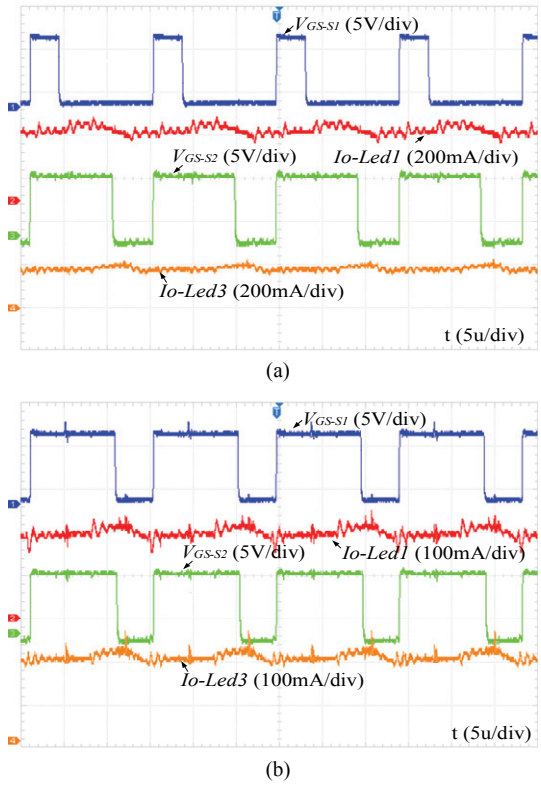

Fig. 14. Independent dimming verification. (a) SCC2 module adjustment; (b) SCC1 and SCC2 module adjustment.

However, LEDs require a current ripple with a maximum variation below 30% to preserve the luminous flux and efficacy [26], where the maximum ripple ($\Delta I_{o\text{-}Led3}$ = 37 mA) of the proposed driver is calculated as 10.3%.

Fig. 14(a) shows that SCC_1 maintains a fixed duty cycle. Therefore, the output current is still approximately 360 mA. Meanwhile, the output current of $I_{o\text{-}Led3}$ is set to approximately 185 mA through the regulation of D_{S2}. Thus, the independent control of the output current is achieved with a wide range of dimming. In another case, SCC_1 and SCC_2 are simultaneously regulated at the same value, where the experimental waveforms are presented in Fig. 14(b). From Fig. 14(b), currents $I_{o\text{-}Led1}$ and $I_{o\text{-}Led3}$ are stable at 185 and 192 mA, respectively. In fact, the capacitor has approximately 5% tolerance. However, as shown in Figs. 14(a) and 14(b), the fluctuation of the output current is small, and the quality of the driving current is remarkably high. Fig. 14(c) shows the start-up waveforms of the four LED strings. After start-up, the current sharing is achieved and consumes a short time, indicating a fast, dynamic response and a good steady current-balancing feature among the four LED channels.

Fig. 15 plots the efficiency for the output current from 160 mA to 400 mA, where the maximum efficiency is 93.8% at 360 mA. In addition, the main loss of the proposed driver is produced in the rectifier unit (diode conduction losses) and the magnetic loss of L_r.

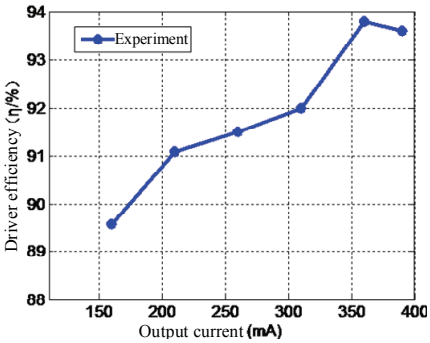

Fig. 15. Efficiency curve of the driver prototype.

VII. Conclusions

A new methodology for independently controlling multichannel LEDs is proposed in this study. The developed control scheme is based on the use of a switching-controlled capacitor in the resonant tank. The capacitance can be regarded as a control parameter for regulating the converter output current. Hence, a constant frequency can be achieved by the proposed solution, thus reducing the size of the EMI filter circuit, which would be high under variable frequency control. To increase the output paths and reduce the cost, the superposition output of the upper and lower half-bridges is proposed. This process achieves excellent performance, where the two fixed capacitors are replaced by SCC_1 and SCC_2 to realize independent dimming. The current sharing scheme and the dimming technique are discussed and employed in the proposed LED driver. A 20 W experimental prototype is debugged for verification. Experimental results show that 1)the accuracy of the multichannel current sharing is high under a large manufacturing error of the LEDs, 2) flicker does not occur due to the small current ripple, and 3) a dimming range of approximately 50% to 110% is implemented.

References

[1] X. Wu, C. Hu, J. Zhang, and Z. Qian, "Analysis and design considerations of LLCC resonant multioutput DC/DC LED driver with charge balancing and exchanging of secondary series resonant capacitors," *IEEE Trans. Power Electron.*, Vol. 30, No. 2, pp.780-789, Feb. 2014.

[2] H. J. Chiu, T. H. Wang and S. C. Mou, "LED backlight driving system for large-scale of LCD panels," *International Conference on Circuits, Signals and Systems*, Vol. 23, No. 3, pp. 166-171, Oct. 2007.

[3] C.-Y. Wu, T.-F. Wu, J.-R Tsai, Y.-M. Chen, and C.-C. Chen, "Multistring LED backlight driving system for LCD panels with color sequential display and area control," *IEEE Trans. Ind. Electron.*, Vol. 55, No.10, pp. 3791-3800, Oct, 2008.

[4] J. Choi, H.-S. Han, and K. Lee, "A current-sourced LED driver compatible with fluorescent lamp ballasts," *IEEE Trans. Power Electron.*, Vol. 30, No. 8, pp. 4455-4466, Aug. 2015.

[5] Y. Lo, K. Wu, K. Pai, and H. Chiu, "Design and implementation of RGB LED drivers for LCD backlight modules," *IEEE Trans. Ind. Electron.*, Vol. 56, No.12, pp. 4862-4871, Dec, 2009.

[6] S. N. Li, W. X. Zhong, W. Chen, and S. Y. R. Hui, "Novel self-configurable current-mirror techniques for reducing current imbalance in parallel light-emitting diode (LED) strings," *IEEE Trans. Power Electron.*, Vol. 27, No. 4, pp. 2153-2162, Apr. 2012.

[7] W.-H. Yang, H.-A. Yang, C.-J. Huang, K.-H. Chen, and Y.-H. Lin, "A high efficiency single-inductor multiple-output buck-type LED driver with average current correction technique," *IEEE Trans. Power Electron.*, Vol. 33, No. 4, pp. 3375-3385, Apr. 2018.

[8] K .I. Hwu, W. C. Tu, and M. J. Hong, "A dimmable LED driver based on current balancing transformer with magnetizing energy recycling considered," *J. Display Technol.*, Vol. 10, No.5, pp. 388-395, May 2014.

[9] R. Zhang and S. H. Chung, "Use of daisy-chained transformers for current-balancing multiple LED strings," *IEEE Trans. Power Electron.*, Vol. 29, No. 3, pp. 1418-1433, Feb. 2014.

[10] E. Asa, K. Colak, M. Bojarski, and D. Czarkowski, "Asymmetrical duty-cycle and phase-shift control of a novel multiport CLL resonant converter," *IEEE J. Emerg. Sel. Topics Power Electron.*, Vol. 3, No. 4, pp. 1122-1131, Mar. 2015.

[11] X. Liu, Q. Yang, Q. Zhou, J. Xu. and G. Zhou, "Single-stage single-switch four-output resonant LED driver with high power factor and passive current balancing," *IEEE Trans. Power Electron.*, Vol. 32, No. 6, pp. 4566-4576, Jun. 2017.

[12] X. Qu, H. H, S. C. Wong, K.T. Chi, and W. Chen, "Hybrid IPT topologies with constant current or constant voltage output for battery charging applications," *IEEE Trans. Power Electron.*, Vol. 30, No. 11, pp. 6329-6337, Jan. 2015.

[13] X. Chen, D. Huang, Q. Li, and F. C. Lee, "Multichannel LED driver with CLL resonant converter," *IEEE J. Emerg. Sel. Topics Power Electron.*, Vol. 3, No.3, pp. 589-598, Sep. 2015.

[14] X.-K Wu, C. Hu, J.-M Zhang, and C. Zhao, "Series–parallel autoregulated charge-balancing rectifier for multioutput light-emitting diode driver," *IEEE Trans. Ind. Electron.*, Vol. 61, No. 3, pp. 1262-1268, Mar. 2014.

[15] Z. Hu, Y. Qiu, Y.-F. Liu, and P.-C. Sen, "A control strategy and design method for interleaved LLC converters operating at variable switching frequency," *IEEE Trans. Power Electron.*, Vol. 29, No. 8, pp. 4426-4437, Aug. 2014.

[16] J. M. Alonso, M. S. Perdigão, D. G. Vaquero, A. J. Calleja, and E. S. Saraiva, "Analysis, design, and experimentation on constant-frequency DC-DC resonant converters with magnetic control," *IEEE Trans. Power Electron.*, Vol. 27, No. 3, pp. 1369-1382, Mar. 2012.

[17] W.-J. Gu and K. Harada, "A new method to regulate resonant converters," *IEEE Trans. Power Electron.*, Vol. 3, No. 4, pp. 430-439, Feb. 1988.

[18] J.-F. Liu, H.-L. Tian, and J. Zeng, "Multi-channel LED driver based on switched-controlled capacitor with constant frequency control," *IET Power Electron.*, Vol. 11, No. 12, pp. 1991-1999, Oct. 2018.

[19] C. S. Wong, K. H. Loo, Y. M. Lai, M. H. L. Chow, and K. T. Chi, "Accurate capacitive current balancing in multistring LED lighting systems based on switched-capacitor-controlled LCC resonant network," *IEEE Trans. Power Electron.*, Vol. 32, No. 3, pp. 2167-2179, Mar. 2017.

[20] S. W. Chi, K. H. Loo, H. C. Iu, Y. M. Lai, and M. Chow, "Independent control of multicolour-multistring LED lighting systems with fully switched-capacitor-controlled LCC resonant network," *IEEE Trans. Power Electron.*, Vol. 33, No. 5, pp. 4293-4305, May 2018.

[21] X. Qu, S. C. Wong, and C. K. Tse, "An improved LCLC current-source-output multistring LED driver with capacitive current balancing," *IEEE Trans. Power Electron.,* Vol. 30, No. 10, pp. 5783-5791, Oct. 2015.

[22] Y. Wang, J.M. Alonso, and X. Ruan, "A review of LED drivers and related technologies," *IEEE Trans. Ind. Electron.*, Vol. 64, No. 7, pp. 5754-5765, Jul. 2017.

[23] Z.-Y. Hu, Y. Qiu, L. Wang, and Y.-F. Liu,"A review of LED drivers and related technologies," *IEEE Trans. Power Electron.*, Vol. 29, No. 6, pp. 2931-2943, Jun. 2014.

[24] Z. Hu, Y. Qiu, Y.-F. Liu, and P. C. Sen, "A control strategy and design method for interleaved LLC converters operating at variable switching frequency," *IEEE Trans. Power Electron.*, Vol. 29, No. 8, pp. 4426-4437, Aug. 2014.

[25] K. H. Loo, Y. M. Lai, and C. K. Tse, "Design considerations of a half-bridge LCC inverter with current balancing for AC-LED," *Conference on IEEE Industrial Electronics Society*. Vol. 23, No.3, pp. 4539-4544, Feb. 2012.

[26] R.-L. Lin and Y.-F. Chen, "Equivalent circuit model of light-emitting- diode for system analyses of lighting drivers," *Proc. Industry Applications Society Meeting*, Vol. 22, No.4, pp. 1-5, Jun. 2009.

Guozhuang Liang was born in Baoding, China. He received his B.S. in electrical engineering from Hebei University of Science and Technology, Shijiazhuang, China, in 1991 and his M.S. in electrical engineering from Hebei University of Technology, Tianjin, China, in 1999. He is pursuing his Ph.D. in control engineering at the University of the West of England, Bristol, England, United Kingdom. He joined Hebei University of Science and Technology as Lecturer in the Department of Electrical Engineering in 1997 and became Associate Professor in 2002. He is Professor and Vice Dean in the School of Electrical Engineering at Hebei University of Science and Technology. His current research interests include power electronics applications, electrical detection, and information processing technology.

Hanlei Tian was born in Shijiazhuang, China, in 1992. He started working toward obtaining his M.S. at Hebei University of Science and Technology, Shijiazhuang, China, in 2016 and is studying in the College of Electric Power of the South China University of Technology, Guangzhou, China, for combined training and postgraduate. His current research interests include high-frequency power converter topologies and power factor correction techniques.